



CYCLIC TESTING OF DISSIPATIVE EMBEDDED COLUMN BASE CONNECTIONS FOR STEEL MOMENT-RESISTING FRAMES

H. Inamasu⁽¹⁾, A. De Castro e Sousa⁽²⁾, D. G. Lignos⁽³⁾

⁽¹⁾ Doctoral assistant, École polytechnique fédérale de Lausanne (EPFL), hiroyuki.inamasu@epfl.ch

⁽²⁾ Postdoctoral researcher, École polytechnique fédérale de Lausanne (EPFL), albano.sousa@epfl.ch

⁽³⁾ Associate professor, École polytechnique fédérale de Lausanne (EPFL), dimitrios.lignos@epfl.ch

Abstract

In this paper, we propose a new concept for embedded column base connections specifically applicable to wide flange steel columns in moment-resisting frames (MRFs) designed in seismically prone areas. In the proposed concept, the inelastic deformation is concentrated in the steel column portion embedded to the reinforced concrete (RC) foundation, which contrasts the current design paradigm that typically leads to local buckling of the fixed end column followed by residual axial shortening. The concrete portion of the footing surrounding the steel column restrains the potential local buckling of the dissipative embedded portion. As such, this ensures an overall stable hysteretic behavior of the steel column-RC footing subassembly even at large lateral deformations. Key features of the proposed design concept involve: 1) a steel column flange reduction inside the RC foundation; 2) the steel column is de-bonded from the surrounding concrete with a de-bonding material layer; and 3) the RC foundation is designed so as to remain elastic. Two wide-flange steel column specimens are physically tested at full-scale at the EPFL Structures Laboratory to explore the proposed design concept. One represents the so-called dissipative column base, whereas the other one reflects the current design practice (i.e., designed as weak-column/strong-base connection). The specimens are subjected to symmetric cyclic loading. The experimental results suggest that the proposed design concept may be used to effectively mitigate local buckling at the fixed end column and the associated axial shortening. Current limitations are also discussed.

Keywords: Cyclic testing, Embedded column bases, Wide-flange steel columns, Column axial shortening, Residual deformations.



1. Introduction

In the seismic design of steel moment-resisting frames (MRFs), column base connections are often idealized as fully fixed. Fixed-end steel columns may sustain inelastic flexural deformations during a seismic event due to the kinematics of the steel MRF. Depending on the magnitude of lateral deformations, a fixed end steel MRF column may experience nonlinear geometric instabilities (e.g., local buckling), often coupled with member instabilities (e.g., lateral torsional buckling). Past experimental studies [1]–[4] suggest that nonlinear geometric instabilities induce (1) flexural strength deterioration and (2) column residual axial shortening. Both (1) and (2) become significant as the amount of cumulative inelastic rotation sustained by the column increases [2], [5], [6]. In recent work, it was demonstrated that column axial shortening may also increase the potential for building demolition in the aftermath of earthquakes [7].

In the current practice, fixed base connections are frequently devised as embedded column base (ECB) connections in mid- and high-rise steel MRF buildings. In such a configuration, a steel column is embedded into a reinforced concrete (RC) foundation. When the RC foundation has sufficient strength, the axial and shear force demands of the column are resisted through bearing against the RC foundation [8]–[10]. The flexural demands of the column, from outside to inside the foundation, is largest near the surface of the RC foundation. The bottom portion of the embedded column experiences the lowest flexural demands — This may be idealized as a cantilevered beam loaded at its end and supported by two closely spaced pins. Moreover, friction between the embedded portion of the steel column and the RC foundation somewhat contributes to the overall flexural resistance of the column base connection [11].

Recent experimental studies on ECB connections suggest that the elastic concrete bearing deformation induces a more flexible boundary than the commonly assumed fixed one [8]–[10]. In addition to elastic flexibility, one experiment that focused on the inelastic performance of the concrete footing itself, rather than the steel column, suggests that ECB connections may be able to sustain large inelastic deformations under cyclic loading [8]. Special attention should be given to the effects of column base flexibility, since they can be instrumental in determining the overall structural behavior along with governing failure modes [12]. Furthermore, past numerical studies suggest that column axial shortening can be minimized when the column base connection sustains part of the inelastic rotation demands [13]–[15].

This paper proposes a new dissipative ECB connection design concept specifically tailored for wide-flange steel columns of MRFs. The new design concept ensures (a) a non-degrading hysteretic response of the steel column/RC footing subassembly even at large inelastic deformations and (b) the mitigation of column axial shortening (following [13]–[15]). This is achieved by (1) mobilizing the steel column portion embedded in the RC footing, rather than the portion above the foundation, and (2) restraining the potential local instability of the embedded portion of the steel column with the presence of the surrounding concrete. The proposed concept is validated by physical quasi-static reversed cyclic tests conducted at the EPFL Structures Laboratory. An additional test of the current design paradigm is conducted for comparison purposes.

2. Experimental Program

2.1 Description of test specimens

The effectiveness of the proposed dissipative ECB concept is investigated by comparing it with a conventional ECB. Two ECB specimens are designed and constructed: 1) the conventional one and 2) the proposed dissipative ECB. The two specimens are nominally identical except for the details of the embedded part of the steel column. Shown in figure 1 is an overview of the test specimen (conventional ECB). The primary geometric properties along with the steel/concrete material type are indicated in figure 1. Each specimen consists of a cantilever steel column welded to a steel plate. The welded end is embedded into the RC foundation. An IPE400 (nominal dimension: depth $d = 400\text{mm}$, width $b_f = 180\text{mm}$, web thickness $t_w = 8.6\text{mm}$, flange thickness $t_f = 13.5\text{mm}$) (web local slenderness $h/t_w = 38.5$, flange local slenderness $b_f/2t_f = 6.7$) with a total length of 2575mm, including an embedment depth of 850mm, is adopted. The 500mm x 280 mm base plate with 30mm thickness is employed. The column and the base plate are welded with a complete joint



penetration without any special weld requirements. The concrete block has a footprint of 1885 x 685mm and a height of 1075mm. The concrete reinforcement is shown in the figure 1.

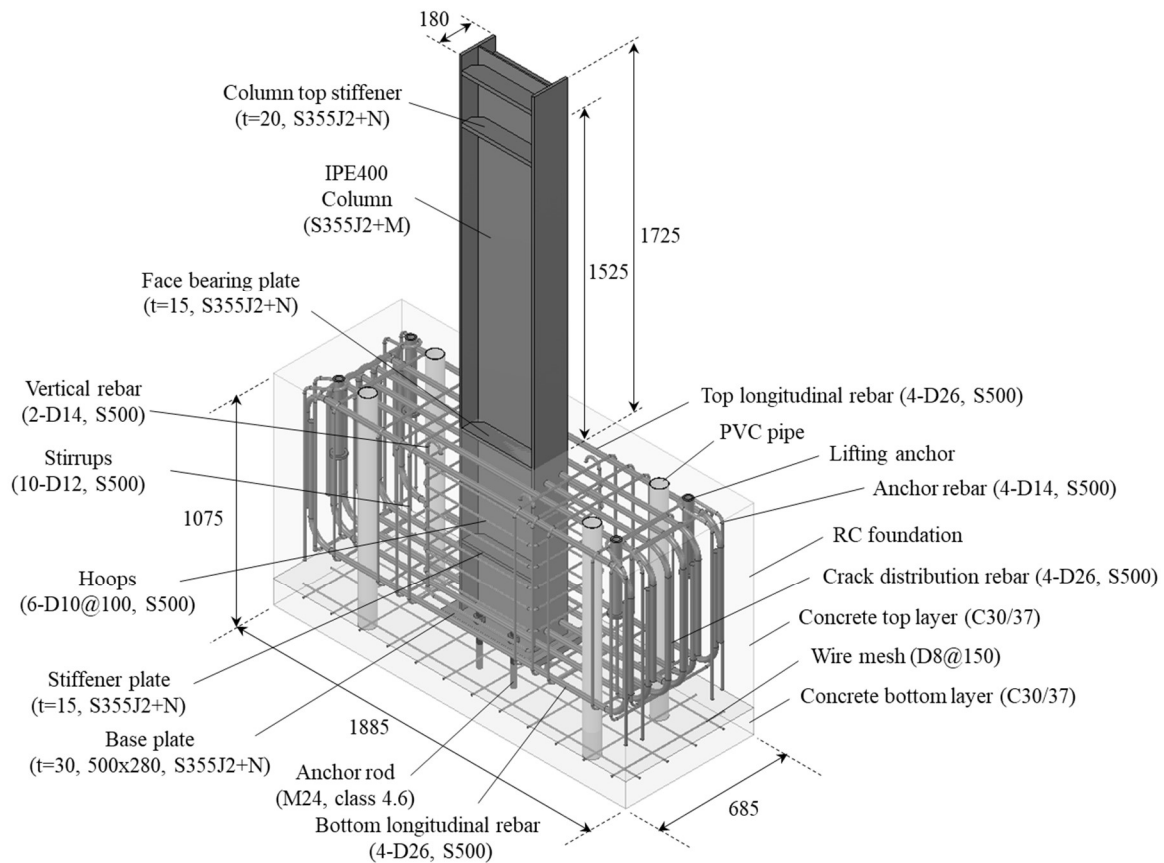


Fig. 1 – Overview of typical specimen (unit: mm)

The conventional ECB specimen is mainly devised according to the current American seismic standards [16]–[18] with complemented provisions from Europe [19] and Japan [20]. The RC foundation is designed to remain elastic. Referring to figure 1, conventional embedded column base connections feature face bearing plates as well as stiffeners to somewhat ensure the fixed end boundary.

In the specimen fabrication, a concrete block is casted separately in two layers. The bottom layer is 125mm thick and is cast containing within itself four positioning anchor rods, a wire mesh and four polyvinyl chloride (PVC) pipes. The anchor rods protrude from the bottom layer and are used to level the column together with leveling nuts in a subsequent stage. The wire mesh prevents concrete cracking due to shrinkage. The PVC pipes are placed in order to have four inserts along the concrete block height, such that tie down anchors can pass through the foundation and fix the specimen to the test setup. The top concrete layer is 950 mm thick, bringing the total height to approximately 1.1 meter. The steel columns are installed vertically on the foundation and rest atop leveling nuts screwed onto the four protruding shallow anchors. These nuts are not tightened such that the contribution of the anchor rods to the flexural resistance is minimized. Reinforcing bars are assembled outside the casting formwork to form a cage. Once the rebar cage is built, it is installed inside the formwork from the top.

In the dissipative ECB specimen, the face bearing plates and stiffeners are not adopted. Moreover, the steel column portion inside the RC foundation is reduced in the flanges. A 3mm thick de-bonding material layer wraps around the embedded part of the steel column, such that the concrete is decoupled from the inelastic



flexural deformation participation. These conditions ensure that the inelastic deformations concentrate in the reduced portion inside the RC footing.

Table 1 summarizes the measured material properties for both steel and concrete; f_y and f_u are the measured yield and tensile stress of the steel parts, respectively, including the steel rebars that are used for the steel reinforcement inside the RC footing; f_c is the 28-day compressive stress of the concrete. Because concrete casting is done in two stages, the compressive stress of both the bottom and top layers is reported in Table 1.

Table 1 – Primary material properties of employed steel/concrete (unit: MPa)

Steel (f_y ; f_u)							Concrete (f_c)	
IPE400		Base plate	Rebars				Bottom	Top
Web	Flange		D26	D14	D12	D10		
407.4;504.4	393.2;489.4	372.7;550.7	522.3;645.3	507.3;584.8	500.0;584.3	552.0;657.0	49.1	47.6

2.2 Test apparatus, imposed loading protocol and instrumentation

Figure 2 illustrates the elevation views of the test apparatus. Only lateral load is applied to the specimens through a 1000kN servo-hydraulic actuator, which is mounted on a transverse beam. The beam is connected to a reaction system comprising two braced frames that transfer the horizontal load imposed by the actuator to the strong floor. A specimen is placed on a spreader beam that is fixed on the strong floor. The specimen is fixed on the spreader beam with four pre-tensioning rods (700kN per rod) that are inserted into the four PVC pipes, which are running through the RC footing as shown in figure 1. Two shear keys are placed on each side of the RC foundation, such that any potential slip of the specimen on the spreader beam is prevented. The specimen's top end is mounted on the actuator swivel through a rigid plate with pre-tensioning rods. Referring to figure 2, the nominal effective cantilever height of the column (i.e., the distance from the top surface of the RC foundation to the actuator loading line) is 1525mm.

The specimen is restrained laterally by a lateral support system. This consists of two running wide-flange beams mounted on four vertical posts (see figure 2). The running beams are placed 860mm higher than the RC foundation top surface. The specimen slides against the running beams on greased interfaces to minimize potential friction during the lateral movement.

Each specimen is subjected to a standard symmetric cyclic loading protocol [21]. Several linear variable displacement transducers (LVDTs) are employed to monitor potential movement of the test apparatus components. Several strain gauges are also installed in the reaction system in order to check the resisting response of the reaction system. The column tip displacement is measured with two string potentiometers. A three-dimensional digital image correlation (DIC) system is also instrumented in order to make surface strain distribution measurements. This stereo-correlation DIC system consists of a pair of cameras, with a distance of about 500mm between them, installed facing the east side of the column flange. Their line-of-sight is approximately at a 45° angle, with respect to the top face of the foundation (horizontal plane). The cameras are also set up at a distance of approximately 1.2m from their target, the edge that results from the intersection of the east column flange (vertical plane) and the concrete top surface (horizontal plane).

Hereinafter, the base moment is defined as the moment at the top surface of the RC foundation (i.e., lateral load measured by the actuator multiplied by the nominal effective cantilever height of the column). The column drift ratio is defined as the relative column top lateral displacement with respect to the RC foundation centerline divided by the nominal effective cantilever height of the column. The imposed loading towards east is defined to be positive.

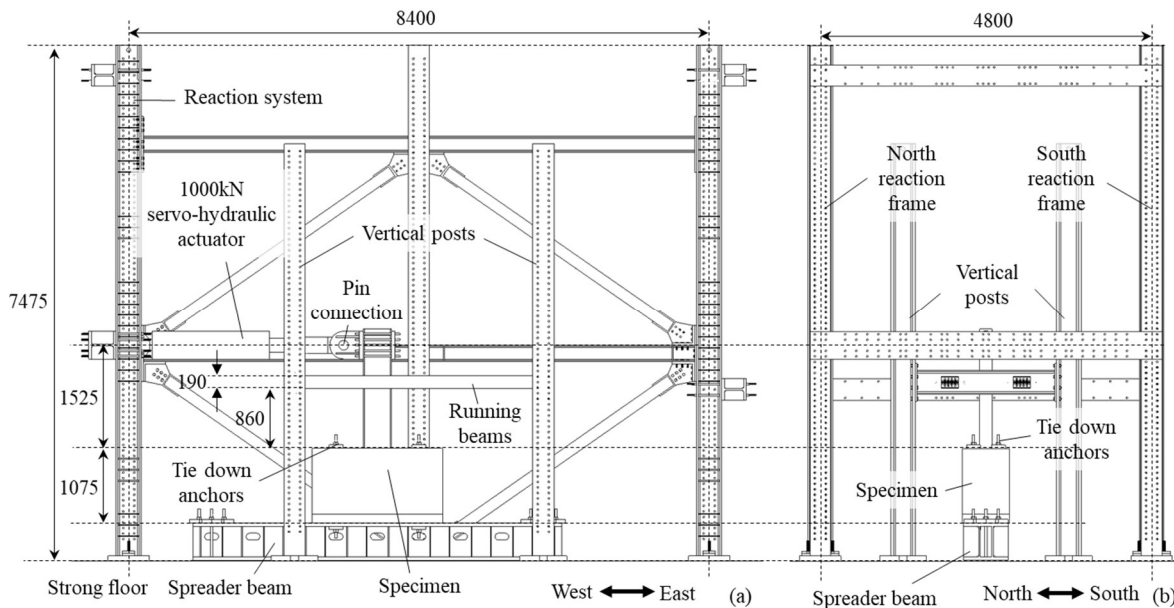


Fig. 2 – Test setup – (a) south elevation (south reaction frame is not shown) and (b) west elevation. Units are in mm.

3. Test Results

3.1 General observations on the cyclic behavior of the test specimens

Figure 3 (a) shows the base moment – column drift ratio relation obtained from the conventional ECB specimen. The elastic rotational stiffness of the base moment – column drift ratio was found to be 48400kNm/rad. During the 0.5% drift amplitude cycles, the cover concrete near the edge of the flanges started cracking. This was caused by the pull-out of each column flange from the foundation while the column deformed laterally. In the course of the 0.75-1% drift amplitude steps, flexural yielding of the column flanges became evident. During the first cycle of the 1.5% drift amplitude, the tangent stiffness decreased significantly, indicating considerable flexural yielding of the respective cross-section. The base moment was around 500kNm. Hairline cracks (less than 0.1mm thick) were identified at the north and south sides of the RC foundation. Until the first cycle of the 4% drift amplitude, a stable moment – rotation relation was observed. At the peak of the 2nd cycle of 4% drift amplitude, the onset of flange local buckling near the RC foundation surface became evident. Cracking (or minor spalling) of the cover concrete near the edge of the column flanges also grew. In the subsequent loading cycle, the local buckle became even more noticeable, a fact that was also flagrant in the severe flexural strength deterioration that was being recorded. Figure 4 (a) shows the deformed shape at the negative peak of the 2nd cycle at the 6% drift amplitude. A considerable amount of inelastic deformation concentrated at the column bottom was evident. During the 6% drift amplitude, tearing was observed near the weld between the face bearing plate and the column (figure 5a). Furthermore, during the 2nd cycle of the 7% drift amplitude, tearing was observed near the k-area in the local buckle region as depicted by figure 5b. The ductile tearing in the k-area grew more in the 7% drift amplitude. The test was terminated at this point. This failure mode was fairly similar with prior cyclic tests on wide-flange steel columns [3]. Cover concrete cracking did not grow after the occurrence of local buckling due to the concentration of the inelastic deformations in the local buckling region. The number of hairline cracks increased after the 1.5% drift amplitude. However, they did not influence the specimen's lateral resistance. The maximum attained base moment was nearly 640kNm during the 2nd cycle of the -4% drift amplitude.

Figure 3 (b) shows the base moment – column drift ratio relation obtained from the dissipative ECB specimen. The elastic rotational stiffness of the base moment – column drift ratio was nearly 25000kNm/rad. This value was nearly half of that from the conventional ECB. This may be attributed to the respective gap due



to the de-bonding material layer. The column base behavior was nearly elastic up to the 0.75-1.0% drift amplitude. From the 0.75-1% drift amplitude cycles, an elastic stiffening behavior was observed. It is noteworthy that the measured stiffness was about 1.5-2.0 times the initial stiffness (comparable to the elastic stiffness of the conventional ECB) due to a shift of the resisting mechanism of the RC foundation. Flexural yielding was evident from the base moment – column drift ratio relation during the 1.5% drift amplitude. The base moment at this point was around 300kNm. Due to the cross-section reduction inside the RC foundation, the flexural strength of the dissipative ECB was about 40% smaller than that of the conventional ECB connection. During the 2% drift amplitude, the concrete cover near the web started cracking. This was possibly caused by the pull-out of the column flange caused by the rotation of the column inside the foundation. However, this remains to be verified after cutting the RC footing. Some hairline cracks were observed at the north and south sides of the RC foundation at the 3% drift amplitude load step. Some additional hairline cracks appeared after the 3% drift amplitude. However, their impact on the specimen's flexural resistance was found to be minor. While the lateral deformation increased from 3 % drift, the cover concrete was increasingly pulled out. Up until the 1st cycle of the 7% drift amplitude, a non-degrading moment – rotation relation was observed while no inelastic deformation of the column above the foundation was observed. This indicates that the proposed dissipative ECB mechanism successfully shifted the inelastic zone inside the RC footing, as anticipated.

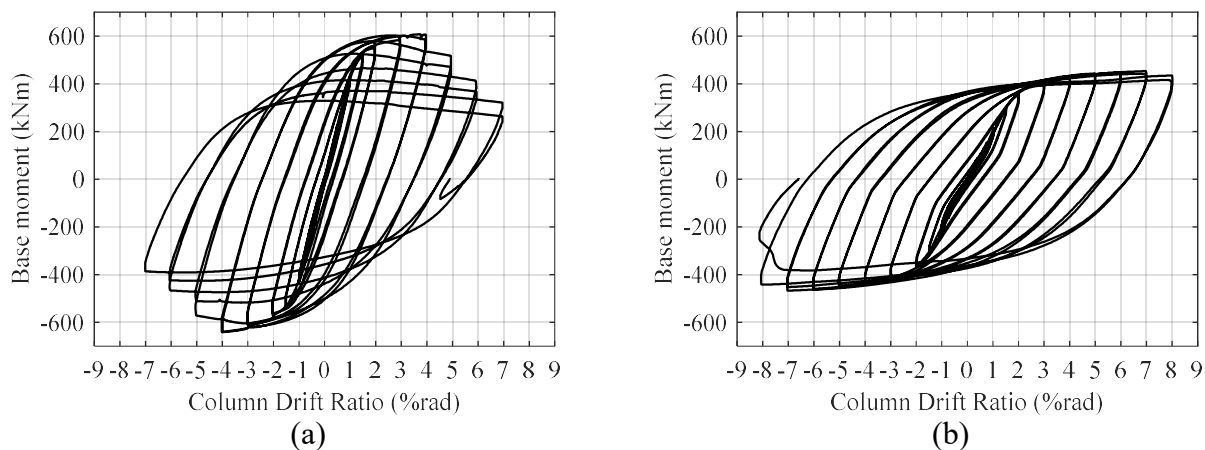


Fig. 3 – Measured base moment – column drift ratio relation: (a) Conventional ECB; (b) Dissipative ECB

Figure 4 (b) shows the deformed shape of the column/footing subassembly at the negative peak of the 2nd cycle of 6% drift amplitude. It is evident that the column above the foundation is “damage-free”. From the 2nd cycle of 7% drift amplitude, minor concentrated local deformations of the flanges were observed. During the 2nd cycle of the 8% lateral drift amplitude, the flexural strength of the test specimen decreased rapidly. Since no fracture was observed outside the foundation, it is speculated that this was due to the inelastic deformation, which was concentrated inside the foundation. Nonetheless, this requires further investigation by cutting the RC footing to further comprehend the corresponding failure mode. This process is currently underway. Overall, the hysteretic behavior of the dissipative ECB was characterized by minor pinching. This may be due to two different bearing mechanisms observed in the elastic range. The maximum attained base moment was slightly above 450kNm (at 1st cycle of -7% drift amplitude).

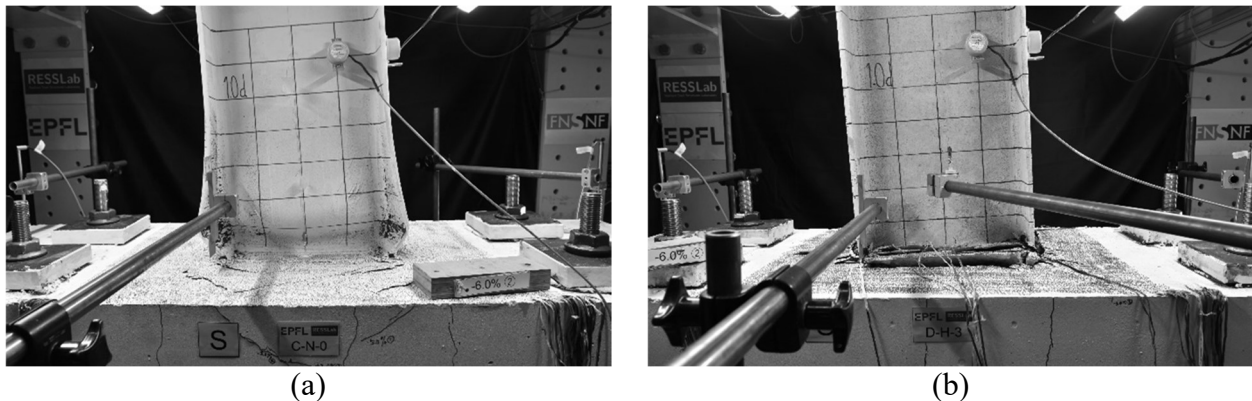


Fig. 4 – Deformation of the specimens at negative peak of 2nd cycle of 6% column drift ratio: (a) Conventional ECB and (b) Dissipative ECB

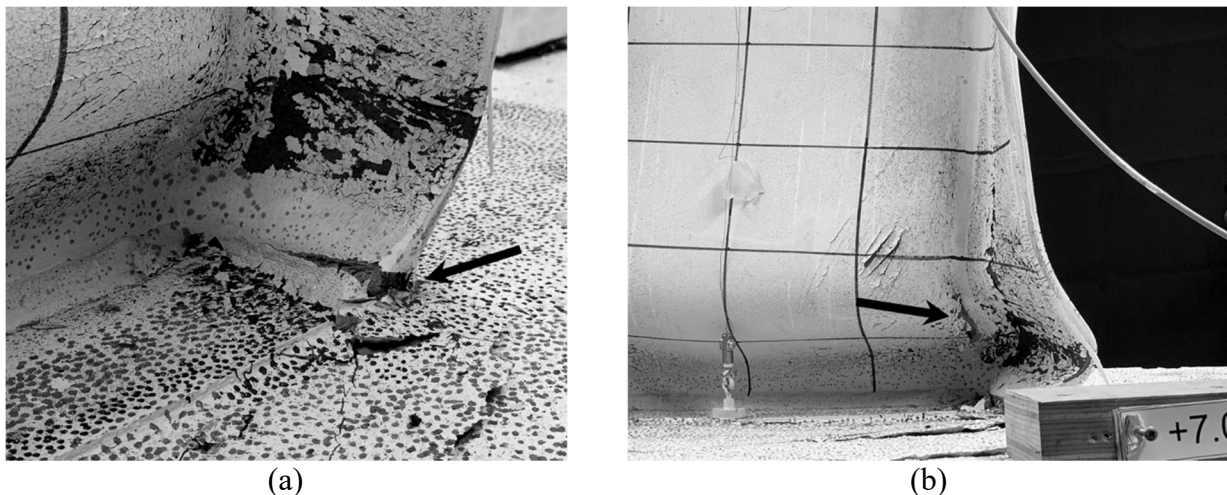


Fig. 5 – Tearing observed in conventional ECB (a) near the weld between the face bearing plate and the column (at positive peak of 2nd cycle of 6% column drift ratio) and (b) near the k-area in the local buckle region (at positive peak of 2nd cycle of 7% column drift ratio)

3.2 Strain field measured with digital image correlation system

With a three-dimensional DIC system, surface strains were measured on the plane of column flanges (vertical) as well as the top surface of the concrete foundation (horizontal). Figures 6 and 7 illustrate the major principal engineering strain fields (ϵ_1) of the east side of the specimens measured with the DIC system. Images taken during the tests were post-processed using the software Vic-3D Digital Image Correlation version 8.0.6 [22]. Positive strain indicates a tension field.

Both strain field images in figure 6 are obtained from the dissipative ECB specimen. They are taken at the peaks of (a) the 1st positive 0.5% and (b) 1st positive 2.0% drift amplitude. In figure 6, the column flange was bearing against the concrete while the column/footing subassembly was undergoing lateral drift demands. During the 0.5% drift amplitude, the strain demand at the concrete surface and the column flange above the foundation was minor, indicating that the column portion inside the RC foundation sustained most of the inelastic strain demands. During the 1.5% drift amplitude, surface cracks on the concrete cover were evident. This was due to the column flange bearing against the RC foundation. The strain demand in the column ranged between 0.1-0.2%. The comparison between figures 6(a) and (b) suggests that, in the initial stiffness range of the dissipative ECB, its lateral resistance mechanism is somewhat different than that of the conventional ECB.



Figure 7 compares the strain fields at the 1st negative 1.5% drift amplitude between the (a) conventional and (b) the dissipative ECBs. In these images, the loading direction is opposite to that of images in figure 6. Referring to figure 7(a), widespread yielding was measured at the column flange surface. On the other hand, as shown in figure 7(b), in the dissipative ECB case, the strain demands of the column portion above the foundation were fairly small (0.1-0.2% strain on the column flange surface). This implies that the inelastic behavior of the specimen likely occurred in the column portion inside the RC foundation.

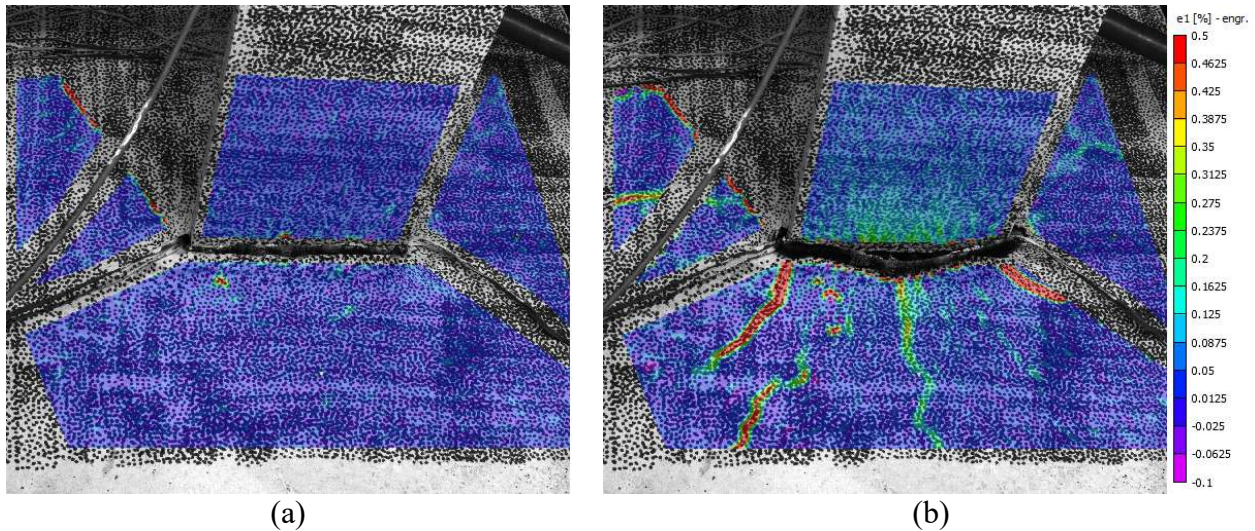


Fig. 6 – Major principal strain fields of the east side of the dissipative ECB observed at the peak of (a) 1st positive 0.5% and (b) 1st positive 2.0% drift amplitude

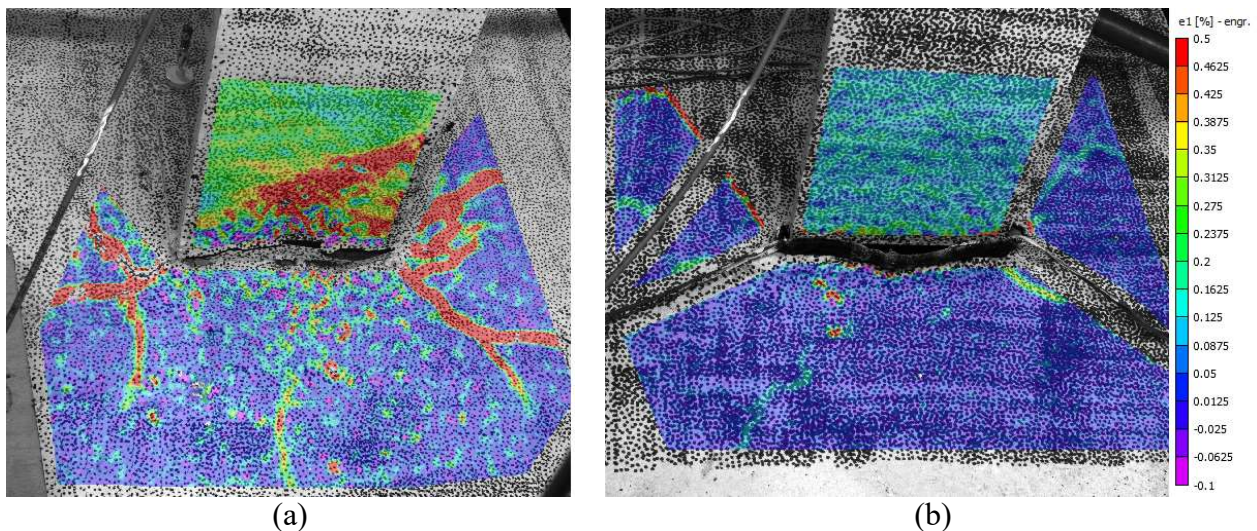


Fig. 7 – Major principal strain fields of the east side of (a) conventional ECB and (b) dissipative ECB observed at the peak of 1st negative 1.5% drift amplitude



4. Conclusions/Limitations

This paper proposed a new embedded column base (ECB) connection design concept that alleviates nonlinear geometric instabilities seen in conventional fixed-type ECBs at inelastic lateral drift demands. In the dissipative ECB concept, the inelastic deformation of the column base is concentrated in the portion of the steel column, which is located inside the foundation. The effectiveness of the dissipative ECB concept was investigated through quasi-static reversed cyclic lateral loading experiments. The test matrix featured a conventional and a dissipative ECB connection. The conventional one reflects the current seismic design practice in fixed-base steel MRF columns. The preliminary findings are summarized as follows,

1. In the conventional ECB, local buckling caused severe flexural strength deterioration of the column after the 4% lateral drift demand. This is likely to be augmented in the presence of compressive axial load demands, which were ignored in the present study. On the other hand, in the dissipative ECB, no strength deterioration was observed up to nearly double lateral drift demands.
2. Dissipative ECBs successfully sustained the flexural deformation demands inside the RC foundation without crushing it while keeping the shear capacity. Although the cover concrete of the RC foundation was damaged, there was no external sign of concrete crushing happening inside the foundation. However, this remains to be verified by actually cutting the RC footing to comprehend the corresponding failure mode inside the foundation. This process is currently underway.
3. A three-dimensional digital image correlation (DIC) system was used to measure the strain field at the top surface of the RC foundation and the column flange surface. The measured strain fields suggest i) that, in the dissipative ECB, the bearing of the column against the foundation was very limited prior to 0.5% lateral drift demands; and ii) the strain values of the column flange above the foundation of the dissipative ECB were much less than those of the conventional ECB. Particularly, the corresponding strains were on the order of 0.1-0.2%, thereby concentrating the inelastic deformation in the steel column portion inside the RC footing.

A more thorough investigation of the tested specimens is currently underway by the authors.

5. Acknowledgements

This study is based on work supported by the Swiss National Science Foundation (Award No. 200021_169248). The financial support is gratefully acknowledged. Any opinions, findings, and conclusions or recommendations expressed in this paper are those of the authors and do not necessarily reflect the views of sponsors. The authors would like to sincerely thank the personnel of the structural laboratory GIS in EPFL (Mr. Gérald Rouge and Mr. Gilles Guignet), Mr. Nitesh Karmacharya (former visiting engineer of EPFL), Mr. Elias Merhi (master student of EPFL), Mr. Cesar Ramirez (former summer student at EPFL from the university of Texas at El Paso) for their invaluable assistance in conducting the experiment series.

6. References

- [1] Elkady A, Lignos DG (2018): Full-Scale Testing of Deep Wide-Flange Steel Columns under Multiaxis Cyclic Loading: Loading Sequence, Boundary Effects, and Lateral Stability Bracing Force Demands. *Journal of Structural Engineering*, **144**(2), 04017189.
- [2] Cravero J, Elkady A, Lignos DG (2020): Experimental Evaluation and Numerical Modeling of Wide-Flange Steel Columns Subjected to Constant and Variable Axial Load Coupled with Lateral Drift Demands. *Journal of Structural Engineering*, **146**(3), 04019222.
- [3] Suzuki Y, Lignos DG (2015): Large Scale Collapse Experiments of Wide Flange Steel Beam-Columns. *Proceedings of the 8th International Conference on Behavior of Steel Structures in Seismic Areas (STESSA)*, Shanghai, China.
- [4] Ozkula G, Harris J, Uang C-M (2017): Observations from Cyclic Tests on Deep, Wide-Flange Beam-Columns. *Engineering Journal*, **1**, 45–59.



- [5] MacRae GA, Carr AJ, Walpole WR (1990): The Seismic Response of Steel Frames. Department of Civil Engineering, University of Canterbury, Christchurch, New Zealand, Research Report 90-6.
- [6] Elkady A, Lignos DG (2018): Improved Seismic Design and Nonlinear Modeling Recommendations for Wide-Flange Steel Columns. *Journal of Structural Engineering*, **144**(9), 04018162.
- [7] Elkady A, Güell G, Lignos DG (2019): Proposed methodology for building-specific earthquake loss assessment including column residual axial shortening. *Earthquake Engineering & Structural Dynamics*.
- [8] Grilli DA, Jones R, Kanvinde AM (2017): Seismic Performance of Embedded Column Base Connections Subjected to Axial and Lateral Loads. *Journal of Structural Engineering*, **143**(5), 04017010.
- [9] Nakashima S, Igarashi S (1986): Behavior of Steel Square Tubular Column Bases for Interior Columns Embedded in Concrete Footings under Bending Moment and Shearing Force Part 1: Test program and Load-displacement relationships. *Journal of Structural and Construction Engineering (Transactions of AIJ) (In Japanese)*, (366), 106–118.
- [10] Nakashima S, Igarashi S (1987): Behavior of Steel Square Tubular Column Bases for Interior Columns Embedded in Concrete Footings under Bending Moment and Shearing Force : Part 2 Initial stiffness, ultimate strength and mechanism of stress flow. *Journal of Structural and Construction Engineering (Transactions of AIJ) (In Japanese)*, (374), 63–76.
- [11] Takeda T, Takahashi Y (1982): Experimental Study on the Column Base of Steel Structure and Steel Reinforced Concrete Structure Part 2: Examination of the Interior Embedded Column Bases. *Summary of Technical Papers of Annual Meeting, Kanto Branch (In Japanese)*, (53), 229–232.
- [12] Aviram A, Stojadinović B, Der Kiureghian A (2010): *Performance and reliability of exposed column base plate connections for steel moment-resisting frames*. University of California, Berkeley, Pacific Earthquake Engineering Research Center.
- [13] Inamasu H, Kanvinde AM, Lignos DG (2019): Seismic Stability of Wide-Flange Steel Columns Interacting with Embedded Column Base Connections. *Journal of Structural Engineering*, **145**(12), 04019151.
- [14] Inamasu H, Lignos DG (2019): Concepts to Minimize Earthquake-Induced Column Axial Shortening in Steel Moment-Resisting Frames. *Proceedings of 12th Pacific Structural Steel Conference*, Tokyo, Japan.
- [15] Inamasu H, Lignos DG, Kanvinde AM (2018): Influence of Embedded Steel Column Base Strength on Earthquake-Induced Residual Deformations. *Proceedings of 16th European Conference on Earthquake Engineering*, Thessaloniki, Greece.
- [16] AISC (2016): *Seismic Provisions for Structural Steel Buildings. ANSI/AISC 341-16*. American Institute of Steel Construction.
- [17] AISC (2016): *Specification for Structural Steel Buildings. ANSI/AISC 360-16*. American Institute of Steel Construction.
- [18] AISC (2012): *Seismic Design Manual. 2nd Edition*. American Institute of Steel Construction.
- [19] CEN (2004): *Eurocode 2 Design of concrete structures - Part 1-1: general rules and rules for buildings*. .
- [20] AIJ (2012): *Recommendations for Design of Connections in Steel Structures, 3rd edition*. Architectural Institute of Japan.
- [21] Clark PW, Frank K, Krawinkler H, Shaw R (2002): *Protocol for Fabrication, Inspection, Testing and Documentation of Beam-column Connection Tests and Other Experimental Specimens*. SAC Joint Venture.
- [22] Vic-3D (2018): *Vic-3D Digital Image Correlation Program*. South Carolina: Correlated Solutions, Inc.